Tubular Anisotropy Segmentation

Fethallah Benmansour and Laurent D. Cohen
{benmansour, cohen}@ceremade.dauphine.fr

CEREMADE, UMR CNRS 7534, Université Paris Dauphine, Place du Maréchal De Lattre De Tassigny, 75775 PARIS CEDEX 16 - FRANCE

Abstract. In this paper we present a new interactive method for tubular structure extraction. The main application and motivation for this work is vessel tracking in 2D and 3D images. The basic tools are minimal paths solved using the fast marching algorithm. This allows interactive tools for the physician by clicking on a small number of points in order to obtain a minimal path between two points or a set of paths in the case of a tree structure. Our method is based on a variant of the minimal path method that models the vessel as a centerline and surface. This is done by adding one dimension for the local radius around the centerline. The crucial step of our method is the definition of the local metrics to minimize. We have chosen to exploit the tubular structure of the vessels one wants to extract to built an anisotropic metric giving higher speed on the center of the vessels and also when the minimal path tangent is coherent with the vessel's direction. This measure is required to be robust against the disturbance introduced by noise or adjacent structures with intensity similar to the target vessel. We obtain promising results on noisy synthetic and real 2D and 3D images.

1 Introduction

In this paper we deal with the problem of finding a complete segmentation of tubular structures like vessels. The main objective is to extract at the same time the centerline of the tubular structure and its boundary. During the last two decades, the extraction of vascular objects such as the blood vessel, coronary artery, or other tube-like structures has attracted the attention of more and more researchers. Various methods such as vascular image enhancement methods [1–3], or others were proposed, see [4] for a complete survey. Some of these methods extract the vessel boundary directly, and then use thinning methods to find its centerline. Other methods extract only the centerline and then estimate the vessel width to extract its boundary. Deschamps and Cohen [5] proposed to use the minimal path method to find the centerline. The minimal path technique introduced by Cohen and Kimmel [6] captures the global minimum curve between two points given by the user. This leads to the global minimum of an active contour energy. Since then, the minimal path method has been improved by many researchers, and adapted to anisotropic media as done by Jbabdi et al for *tractography* [7]. Unfortunately, despite their numerous advantages, classical minimal path techniques exhibit some disadvantages. First, vessel boundary

extraction can be very difficult, even in 2D where the vessel's boundary can be completely described by two curves. Second, the path given by the minimal path technique does not always yield to the centerline of the vessel. A readjustment step is required to obtain a central trajectory. Third, the minimal path technique provides only a trajectory and does not give information about the vessel boundary and local width.

Li and Yezzi [8] proposed a new variant of the classical, purely spatial, minimal path technique by incorporating an extra *non-spatial* dimension into the search space. Each point of the 4D path (after adding the extra dimension for the 3D image) consists of three spatial coordinates plus a fourth coordinate which describes the vessel thickness at that corresponding 3D point. Thus, each 4D point represents a sphere in 3D space, and the vessel is obtained by taking the envelope of these spheres as we move along the 4D curve. A crucial step of this method is to build an adequate potential that drives the propagation. Li and Yezzi [8] proposed different isotropic potentials. As they said in the conclusion of their paper, the proposed potentials are very parameter dependent and they hoped to find more appropriate choice of potential. In particular, one can see in their paper, that the potential used does not yield to a correct detection of the radius when it is not constant (see figure 6 in [8]). An other drawback of Li and Yezzi method is that they did not take into account the vessel orientation. Our first contribution is to take into account the vessel orientation by defining a suited anisotropic metric that makes the propagation faster along the centerlines and for the adequate radius. Law et al. [9] proposed a new scalar descriptor called *Optimally Oriented Flux* (OOF) for the detection of curvilinear structures. But they did not exploit the orientation given by their descriptor. The major advantage of the OOF technique is that it does not consider the regions in the vicinity of target objects, where background noise or adjacent structures with intensity similar to the target vessels are possibly present. Therefore, the disturbance introduced by the closely located nearby structures is avoided. The second contribution of this paper is to build an anisotropic metric based on the OOF descriptor, its scalar function as well as its orientation. That makes the propagation faster along the vessels center line and for exact associated scale. This means that the path location, orientation and scale (radius) have to be coherent with the local geometry of the image extracted by the OOF.

In section 2, we give some background on minimal path method and Anisotropic Fast Marching. In section 3 the Optimally Oriented Flux descriptor is presented as well as the metric construction. In section 4, results on synthetic and real data are shown. Finally, conclusions and perspectives follow in section 5.

2 Background on Minimal Path Method

A minimal path, first introduced in the isotropic ($\mathcal{P}$ does not depend on the orientation of the path) case [6], is a pathway minimizing the energy functional,

$$E(\gamma) = \int_{\gamma} \mathcal{P}\big(\gamma(s), \gamma'(s)\big)\mathrm{d}s \tag{1}$$

where, $\mathcal{P}(\gamma(.),\gamma'(.)) = \sqrt{\gamma'(.)^T \mathcal{M}(\gamma(.))\gamma'(.)}$ describes an infinitesimal distance along a pathway γ relative to a metric tensor $\mathcal{M}$ (symmetric definite positive). Thus, we are considering only the case of an elliptic medium. In the isotropic case $\mathcal{M}(.) = \mathcal{P}^2(.)I$, where I is the identity matrix. A curve connecting $\mathbf{p}_1$ to $\mathbf{p}_2$ that globally minimizes the above energy (1) is a *minimal path* between $\mathbf{p}_1$ and $\mathbf{p}_2$, noted $\mathcal{C}_{\mathbf{p}_1,\mathbf{p}_2}$.

The solution of this minimization problem is obtained through the computation of the *minimal action map* $\mathcal{U} : \Omega \to \mathbb{R}^+$ associated to $\mathbf{p}_1$ on the domain Ω which can be a 2D, 3D or 4D domain. The minimal action is the minimal energy integrated along a path between $\mathbf{p}_1$ and any point $\mathbf{x}$ of the domain Ω :

$$\forall\ \mathbf{x} \in \Omega,\ \mathcal{U}(\mathbf{x}) = \min_{\gamma \in \mathcal{A}_{\mathbf{p}_1,\mathbf{x}}} \left\{ \int_\gamma \mathcal{P}\big(\gamma(s),\gamma'(s)\big)\mathrm{d}s \right\}, \tag{2}$$

where $\mathcal{A}_{\mathbf{p}_1,\mathbf{x}}$ is the set of paths linking $\mathbf{x}$ to $\mathbf{p}_1$. The values of $\mathcal{U}$ may be regarded as the arrival times of a front propagating from the source $\mathbf{p}_1$ with oriented velocity related to the metric tensor $\mathcal{M}^{-1}$. $\mathcal{U}$ satisfies the Eikonal equation

$$\|\nabla\mathcal{U}(\mathbf{x})\|_{\mathcal{M}^{-1}(\mathbf{x})} = 1 \text{ for } \ \mathbf{x} \in \Omega, \text{ and } \mathcal{U}(\mathbf{p}_1) = 0, \tag{3}$$

where $\|\mathbf{v}\|_M = \sqrt{\mathbf{v}^T M \mathbf{v}}$. The map $\mathcal{U}$ has only one local minimum, the point $\mathbf{p}_1$, and its flow lines satisfy the Euler-Lagrange equation of functional (1). Thus, the minimal path $\mathcal{C}_{\mathbf{p}_1,\mathbf{p}_2}$ can be retrieved with a simple gradient descent on $\mathcal{U}$ from $\mathbf{p}_2$ to $\mathbf{p}_1$ (see Fig. 1), solving the following ordinary differential equation with standard numerical methods like Heun's or Runge-Kutta's :

$$\frac{\mathrm{d}\mathcal{C}_{\mathbf{p}_1,\mathbf{p}_2}}{\mathrm{d}s}(s) \propto -\mathcal{M}^{-1}(\mathcal{C}_{\mathbf{p}_1,\mathbf{p}_2}(s))\nabla\mathcal{U}\big(\mathcal{C}_{\mathbf{p}_1,\mathbf{p}_2}(s)\big), \text{ with } \mathcal{C}_{\mathbf{p}_1,\mathbf{p}_2}(0) = \mathbf{p}_2. \tag{4}$$

Proof of (3) and (4) can be found in [10, 7]. On figure 1, we show some examples

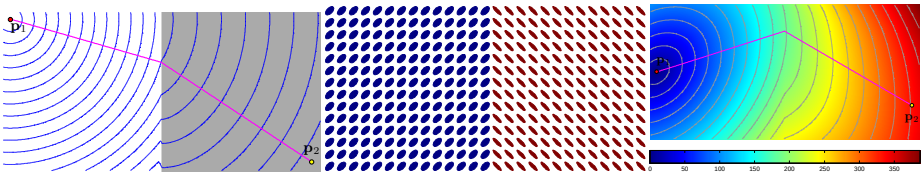

Fig. 1. Minimal path examples on an isotropic case on the left image. On the middle, visualization by small ellipses of eigenvalues of a metric constant on each half side of the image. On the right, the minimal action map associated to the source point $\mathbf{p}_1$ with the minimal path $\mathcal{C}_{\mathbf{p}_1,\mathbf{p}_2}$.

of the minimal path method on an isotropic case and an anisotropic one. On the first image of figure 1 the metric is isotropic and the potential $\mathcal{P}$ in the grey region is twice as low as the white one. Isolevel sets of the minimal action map

associated to the source point $\mathbf{p}_1$ are displayed and so the minimal path $\mathcal{C}_{\mathbf{p}_1,\mathbf{p}_2}$. The second image represents a metric $\mathcal{M}$. We took two constant metrics in each half side of the image with different orientations. On the last image, the minimal action map $\mathcal{U}$ associated to the metric $\mathcal{M}$ and to the source point $\mathbf{p}_1$ is shown. The minimal path $\mathcal{C}_{\mathbf{p}_1,\mathbf{p}_2}$ is found by solving equation (4).

The *Fast Marching Method* (FMM) is a numerical method introduced by Sethian in [11] and Tsitsiklis in [12] for efficiently solving the isotropic Eikonal equation on a cartesian grid. The central idea behind the FMM is to visit grid points in an order consistent with the way wavefronts of constant action propagate. It leads to a single-pass algorithm for solving equation (3) and computing the minimal action map $\mathcal{U}_1$. Tsitsiklis's method relies on minimizing directly the energy functional of equation (1) while Sethian's method uses the Eikonal equation. Both methods are suitable for isotropic metric, but they fail for anisotropic metric [13]. To deal with anisotropy, Sethian and Vladimirsky [10] proposed an update scheme that converges to the viscosity solution of the anisotropic Eikonal equation. A simplified scheme, based on the original Tsitsiklis's method [12], was proposed by Lin in [14] to approximate the solution of the anisotropic Eikonal equation. Contrary to Sethian and Vladimirsky's ordered upwind method (OUM) [10], Lin's algorithm does not converge to the viscosity solution of the Eikonal equation. In this paper we used Lin's scheme to solve the anisotropic Eikonal equation, since it is much faster (than OUM) and the introduced errors does not affect much the extracted geodesics.

The FMM is a front propagation approach that computes the values of $\mathcal{U}$ in increasing order, and the structure of the algorithm is almost identical to Dijkstra's algorithm for computing shortest paths on graphs [15]. In the course of the algorithm, each grid point is tagged as either *Alive* (point for which $\mathcal{U}$ has been computed and frozen), *Trial* (point for which $\mathcal{U}$ has been estimated but not frozen) or *Far* (point for which $\mathcal{U}$ is unknown). The set of *Trial* points forms an interface between the set of grid points for which $\mathcal{U}$ has been frozen (the *Alive* points) and the set of other grid points (the *Far* points). This interface may be regarded as a set of fronts expanding from each source until every grid point has been reached. Let us denote by $\mathcal{N}_{\mathrm{M}}(\mathbf{x})$ the set of M neighbors of a grid point $\mathbf{x}$, where $\mathrm{M} = 2 \times d$ if the dimension of Ω is equal to d. Initially, all grid points are tagged as *Far*, except the source point $\mathbf{p}_1$ that is tagged as *Trial*. At each iteration of the FMM one chooses the *Trial* point with the smallest $\mathcal{U}$ value, denoted by $\mathbf{x}_{\min}$. Then, $\mathbf{x}_{\min}$ is tagged as *Alive* and the value of $\mathcal{U}$ is updated for each point of the set $\mathcal{N}_{\mathrm{M}}(\mathbf{x}_{\min})$ which is either *Trial* or *Far*. In order to satisfy a causality condition, the way $\mathcal{U}$ is updated in the vicinity of $\mathbf{x}_{\min}$ requires special care. The iteration ends by tagging every *Far* point of the set $\mathcal{N}_{\mathrm{M}}(\mathbf{x}_{\min})$ as *Trial*. The algorithm automatically stops when all grid points are *Alive*. The key to the speed of the FMM is the use of a priority queue to quickly find the *Trial* point with the smallest $\mathcal{U}$ value. If *Trial* points are ordered in a min-heap data structure, the computational complexity of the FMM is $\mathcal{O}(N\log N)$, where N is the total number of grid points.

A crucial step of the Fast Marching algorithm is the computation of the weighted distance between the front and the neighbouring voxels in the *Trial* set. Here, we present a way to estimate this weighted distance in the anisotropic case and only in 3D. It is straightforward to extend it to 4D. Since the distance is anisotropic, we cannot use the standard methods, because they rely on the fact that the geodesics are perpendicular to the level sets of $\mathcal{U}$. To take into account the anisotropy Jbabdi et al [7] and Lin [14] considered a set of simplexes that cover the whole neighbourhood around a voxel of the narrow band. The definition of a simplex neighbouring a point $\mathbf{x}$ is simply a set of three points $(\mathbf{x}_1, \mathbf{x}_2, \mathbf{x}_3)$ that are 26 neighbours of $\mathbf{x}$, defining a triangle that they denote $\overline{\mathbf{x}_1\mathbf{x}_2\mathbf{x}_3}$. There are 48 such triangles around $\mathbf{x}$ for the 26 connexities. To make the update procedure faster, we propose to consider only the simplexes defined by a t-uple of three points of the 6-neighbors of $\mathbf{x}$. There are 8 such triangles (see Fig. 2), and by making this modification, the precision of the algorithm is lower but the algorithm is six times faster. To estimate $\mathcal{U}(\mathbf{x}_\mathrm{m})$, where $\mathbf{x}_\mathrm{m}$ is a neighbor

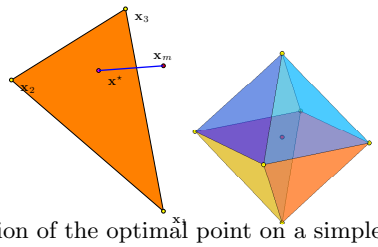

Fig. 2. On the left Position of the optimal point on a simplex such as to minimize the geodesic distance to $\mathbf{x}$. On the right the considered simplexes.

of the last *trial* point $\mathbf{x}_\mathrm{min}$, we make two approximations. If the geodesic passing by $\mathbf{x}_\mathrm{m}$ comes from a triangle $\overline{\mathbf{x}_1\mathbf{x}_2\mathbf{x}_3}$ then the time of arrival is given by :

$$\mathcal{U}(\mathbf{x}_\mathrm{m}) = \min_{\mathbf{x}\in\overline{\mathbf{x}_1\mathbf{x}_2\mathbf{x}_3}} \left\{ \mathcal{U}(\mathbf{x}) + \int_{\mathbf{x}}^{\mathbf{x}_\mathrm{m}} P(\gamma, \gamma') \right\} \tag{5}$$

The term one wants to minimize is approximated by :

$$f(\alpha) = \sum_{i=1}^{3} \alpha_i \mathcal{U}(\mathbf{x}_i) + \left\| \mathbf{x} - \sum_{i=1}^{3} \alpha_i \mathbf{x}_i \right\|_{\mathcal{M}(\mathbf{x})}, \tag{6}$$

where $\alpha = (\alpha_1, \alpha_2, \alpha_3)$, with $\sum_{i=1}^{3} \alpha_i = 1$ since the point $\mathbf{x}$ is in the triangle (see figure 2). This equation follows Tsitsiklis's approximation [12]. The first term approximates the value of the minimal action map at the point $\mathbf{x} = \sum_{i=1}^{3} \alpha_i \mathbf{x}_i$ by a simple linear interpolation. And the second term approximates the remaining distance by considering the metric constant along the segment $[\mathbf{x}, \mathbf{x}_\mathrm{m}]$ equal to its value at point $\mathbf{x}_\mathrm{m}$. The function f is convex and the constraints on α, i.e $\sum_{i=1}^{3} \alpha_i = 1$ and $\alpha_i \geq 0$, define a convex subset. Thus the minimization of f can be done using classical optimization tools. See [7] for more details.

For each of the eight triangles, we get a value u. Finally, we choose the triangle giving the smallest value of u. Note that in order to approximate $\nabla\mathcal{U}$, computing the derivatives of $\mathcal{U}$ in the triangle using the estimate $\mathcal{U}(\mathbf{x}_n)$ gives a consistent approximation of $\nabla\mathcal{U}(\mathbf{x}_\mathrm{n})$ by the following:

$$\nabla\mathcal{U}(\mathbf{x}_\mathrm{n}) = (\mathcal{U}(\mathbf{x}_\mathrm{n}) - \mathcal{U}(\mathbf{x}^\star))\frac{\mathbf{x}_\mathrm{n} - \mathbf{x}^\star}{\|\mathbf{x}_\mathrm{n} - \mathbf{x}^\star\|},$$

where $\mathbf{x}^\star$ is the minimizer of function f, see figure 2 left, and $\|.\|$ is the Euclidean norm. The computation of the gradient is very useful since it is used to solve the gradient descent described by equation (4).

3 Optimally Oriented Flux : an Anisotropy Descriptor

We are interested in the construction of a metric that extracts from the image the geometric information leading to reconstruction of vessels. This means that we wish to find an estimate for the local orientation and scale and a criterion on the local geometry to distinguish the presence of vessels from the background.

At the position $\mathbf{x}$ on an image I, the amount of the image gradient projected along the axis $\mathbf{v}$ flowing out from a 3D sphere (or a 2D circle) S_r is measured as in [9],

$$f(\mathbf{x},\mathbf{v};r) = \int_{\partial S_r} \Big((\nabla(G * I(\mathbf{x}+\mathbf{h}))\cdot\mathbf{v})\mathbf{v}\Big)\cdot\frac{\mathbf{h}}{|\mathbf{h}|}da, \tag{7}$$

where G is a Gaussian function with a scale factor of 1 pixel, r is the sphere (or circle) radius, $\mathbf{h}$ is the position vector along ∂S_r and da is the infinitesimal area (or length) on ∂S_r. To detect vessels having higher intensity than the background region, one would be interested in finding the vessel direction which minimizes $f(\mathbf{x},\mathbf{v};r)$, i.e. we are looking for: $\arg\min_{\mathbf{v}} f(\mathbf{x},\mathbf{v};r)$. Using the divergence theorem, it can be shown that $f(\mathbf{x},\mathbf{v};r)$ can be calculated using a simple convolution,

$$f(\mathbf{x},\mathbf{v};r) = \mathbf{v}^T\ \{(\partial_{i,j}G) * I * \mathbb{1}_{S_r}\}\ \mathbf{v}, \tag{8}$$

where $(\partial_{i,j}G)$ is the Hessian matrix of function G and $\mathbb{1}_{S_r}$ is the indicator function inside the sphere (or circle) S_r. By differentiating the above equation with respect to $\mathbf{v}$, minimization of function f is in turn acquired as solving a generalized eigenvalue decomposition problem. Solving the aforementioned generalized eigen decomposition problem gives d eigenvalues (where $d = 2$ or 3 is the dimension of the image), $\lambda_1(\cdot) \leq \cdots \leq \lambda_d(\cdot)$ and d eigenvectors $\mathbf{v}_i(\cdot)$, i.e. $\lambda_i(\mathbf{x};r) = f(\mathbf{x},\mathbf{v}_i(\mathbf{x};r);r)$ for $i = 1,\ldots,d$. To handle the vessels having various radii, a multi-scale approach should be employed along with the OOF method. In [9], Law and Chung have proposed to normalize the OOF's eigenvalues by the sphere surface area when the OOF method is incorporated in a multi-scale approach for 3D image volumes. In the 2D case the eigenvalues are normalized by the circle perimeter $2\pi r$. In the 3D case the eigenvalues are normalized by the sphere area $4\pi r^2$.

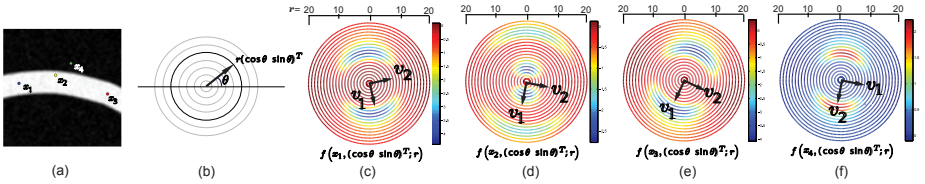

Fig. 3. The plots of the values of $f(\mathbf{x}, \mathbf{v}; r)$ obtained from the synthetic image shown in the left, at four different positions with various radii and projection axes. (a) Four interested positions, denoted as $\mathbf{x}_1$, $\mathbf{x}_2$, $\mathbf{x}_3$ and $\mathbf{x}_4$ are shown along with the original synthetic image. (b) An illustration regarding the polar coordinate system used in (c)-(f). (c)-(f) The plots of the values of $f(\cdot)$ and the corresponding eigenvectors, computed at the four different positions shown in (a), using various values of r and different projection axes $(\cos\theta \;\; \sin\theta)^T$.

In the 2D case (see figure 3), the first eigenvector $\mathbf{v}_1$ represents the direction orthogonal to the vessel for a point on the centerline. $\mathbf{v}_2$ reprensents the direction along the vessel. In the 3D case, if the point is on the centerline, the two eigenvectors associated to the first eigenvalues (λ_1, λ_2) represent the directions orthogonal the vessel. $\mathbf{v}_3$ represents the direction along the vessel, see figure 4. On the same figure, one can see that if the point $\mathbf{x}$ is on the centerline, the minimal response of the function f is obtained when the radius r is equal to the exact radius of the tube. If the point is inside the tube but not on the centerline, $\mathbf{v_3}$ is parallel to the tube orientation, and the other eigenvectors depends on the scale r. If the point is outside the tube (last line), then the vector $\mathbf{v}_3$, corresponding to the red area, is oriented toward the centerline.

Li and Yezzi [8] proposed a new variant of the classical, purely spatial, minimal path technique by incorporating an extra *non-spatial* dimension into the search space. The crucial step of this method is to build an adequate metric that drives the propagation. Li and Yezzi [8] proposed different isotropic potentials. The main drawback, as they mention, is that these potentials are very parameter dependent and they do not exploit the vessel orientation. Our main contribution is to improve Li and Yezzi method by adding to it an anisotropic formulation, and the anisotropic metric is constructed by extension of the OOF descriptor presented by Law et al. [9].

The $(d+1)$D minimal path is found by minimizing the following energy: $\int_\gamma \left\{ \sqrt{\gamma'(s)^T \mathcal{M}(\gamma(s))\gamma'(s)} \right\} \mathrm{d}s$, where $\mathcal{M}$ is the $(d+1)$D anisotropic metric we want to construct. It is not natural to consider anisotropy on the $(d+1)$ dimension, i.e the radii dimension.. Thus one can decompose by block the metric $\mathcal{M}$ as follows: $\mathcal{M}(\mathbf{x}, r) = \begin{pmatrix} \tilde{\mathcal{M}}(\mathbf{x}, r) & 0 \\ 0 & \mathcal{P}_{\text{radii}}(\mathbf{x}, r) \end{pmatrix}$ where $\tilde{\mathcal{M}}(\mathbf{x}, r)$ is a $d \times d$ symmetric definite positive matrix giving the spatial anisotropy and $\mathcal{P}_{\text{radii}}(\mathbf{x}, r)$ is the radii potential (also strictly positive).

Since the result given by the anisotropic minimal path method is very dependent on the metric, results inherit advantages and drawbacks of the constructed

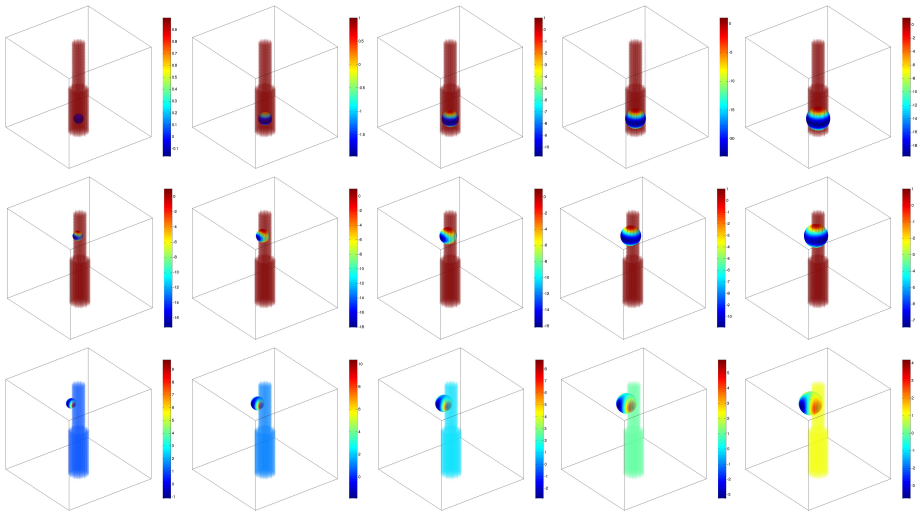

Fig. 4. Plot of $f(\mathbf{x}, \mathbf{v}; r)$ superimposed on the original 3D synthetic image for three different points(on each line) and different values of the radius : $r = 3, \ldots, 7$ from left to right. The radius of the tube on the top half side image is equal to 4, and equal to 6 on the bottom half side. Similarly to figure 3, the visualization of the normalized flux function is done using a spherical coordinate system (instead of the polar one used in 2D). The first point is on the centerline of the tube. The second point is inside the tube but not on the centerline. The third point is outside the tube. The reader should zoom on each image. Notice that the colormaps are different.

metric, thus we should be very carful with its construction. First, let us fix conditions on the desired metric. The spatial metric $\tilde{\mathcal{M}}$ has to be well oriented along the vessel centerline. And the radii potential $\mathcal{P}_{\text{radii}}$ has to be small for the adequate scale for any point of the image. $\mathcal{P}_{\text{radii}}$ corresponds to the inverse speed for the radii dimension. Since $\tilde{\mathcal{M}}$ is symmetric definite positive, we can decompose it as follows: $\tilde{\mathcal{M}}(.) = \sum_{i=1}^{d} m_i(.)\mathbf{u}_i(.)\mathbf{u}_i(.)^T$, where $0 < m_1 \leq \cdots \leq m_d$ are the eigenvalues and $\mathbf{u}_i$ are the associated eigenvectors. The velocity of the propagating front along direction $\mathbf{u}_i$ is equal to $1/\sqrt{m_i}$. We used the OOF descriptor to construct the metric as follows:

$$\tilde{\mathcal{M}}(.) = \sum_{i=1}^{d} \exp\left(\alpha \frac{\sum_{j \neq i} \lambda_j(.)}{d-1}\right) \mathbf{v}_i(.)\mathbf{v}_i(.)^T, \;\; \mathcal{P}_{\text{radii}}(.) = \beta \exp\left(\alpha \frac{\sum_{i=1}^{d} \lambda_i(.)}{d}\right). \tag{9}$$

The constant α is controlled by an intuitive parameter, which is the maximal spatial anisotropy ratio: $\mu = \max_{\mathbf{x},r} \left\{ \frac{\exp(\alpha\lambda_2(\mathbf{x},r))}{\exp(\alpha\lambda_1(\mathbf{x},r))} \right\}$ in the 2D case and $\mu = \max_{\mathbf{x},r} \left\{ \frac{\exp\left(\alpha \frac{\lambda_2(\mathbf{x},r)) + \lambda_3(\mathbf{x},r)}{2}\right)}{\exp\left(\alpha \frac{\lambda_1(\mathbf{x},r)) + \lambda_2(\mathbf{x},r)}{2}\right)} \right\}$ in the 3D case. By choosing the maximal spatial anisotropy ratio μ, the constant α is fixed. And by doing so, the anisotropy

descriptor $\mathcal{M}$ becomes contrast invariant because the OOF is linear on the image. The parameter β controls the radii speed. In 2D (it is very similar in 3D), if $\mathcal{P}_{\text{radii}} \leq \exp(\alpha\lambda_1)$ then the Fast Marching propagation is faster for the radii than the spatial dimensions. If $\mathcal{P}_{\text{radii}} \geq \exp(\alpha\lambda_2)$ then the propagation is slower. One can tune parameter β depending on the tubular structure one wants to extract. If its radius changes a lot then β should be chosen such that the propagation on the radii dimension is faster. If not β is chosen such that the propagation is less sensitive on the radii dimension.

On figure 5 the constructed metric of image 3 at some different scales is shown. Since we chose the same color range for the visualization, we can see that the directions are well detected, and that the optimal values are obtained along the centerline of the tube when the scale is equal to the tube radius. For our experiments, we took $\mu = 10$ and β such that $\max\left(\frac{exp(\alpha\lambda_1)}{\mathcal{P}_{\text{radii}}}\right) = 5$, this means that in the worst situation, the speed along the radii dimension is 5 times faster than the spatial dimensions. We did so, because we want our algorithm to be sensitive on the radii dimension.

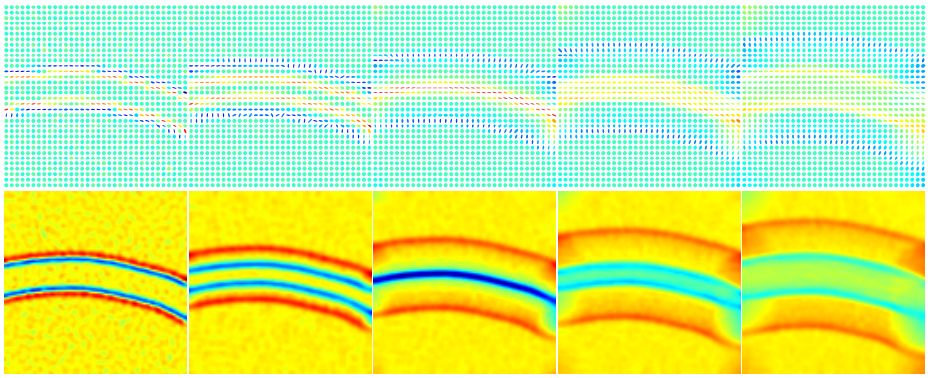

Fig. 5. The constructed metric for different scales $r = 1, 5, 10, 15, 20$ from left to right. The original image is shown in figure 3 (a), the radius of the structure is equal to 10. We used the same color range for all images, so one can see that the optimal anisotropy is obtained along the centerline of the tubular structure when the scale r is equal to the exact radius of the tube. On the top, we show a display of $\tilde{\mathcal{M}}(\mathbf{x}, r)^{-1}$. On the bottom, responses of $\mathcal{P}_{\text{radii}}$ are shown.

4 Experimental Results

Our method is minimally interactive. First, the user has to precise if the desired vessels are darker or brighter than the background. So, we can consider different criteria on signs of the eigenvalues. Then the scale range $[r_{\min}, r_{\max}]$, which corresponds to the range of radii of the vessel one wants to extract, is given by the user. Finally few points are required as source points or end points of the Fast Marching algorithm. We used the metric described in the previous section to find the minimal anisotropic path (as described in section 2) between two or

more selected points (see figures 6 and 7). For any selected point, the associated radius is equal to the minimal radius $r_{\min}$ given by the user.

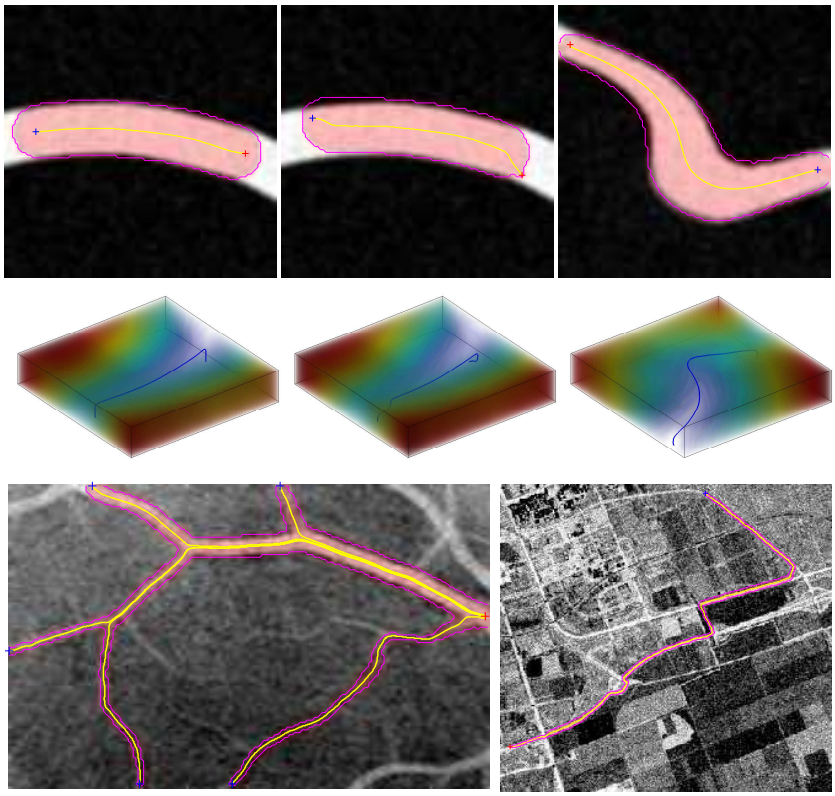

Fig. 6. The red cross points are source points given by the user, and the blue ones are end points. On each case the segmented centerlines are displayed as well as the envelope of the moving discs. In the middle, the associated minimal action map $\mathcal{U}$ as well as the 3D minimal path between the two selected points are shown (transparent visualization).

On figure 6, segmentation results on synthetic and real noisy 2D images are shown. On the first synthetic image, the source point and destination are selected on the centerline. The obtained tube is perfectly detected as well as the centerline. On the second image, the initial points are decentered. But the centerline given by our algorithm goes back fastly to the real centerline. This makes our algorithm robust to initialization. The third synthetic image shows that our approach is robust to scale changing. On the last line of figure 6, segmentation results are shown on real noisy images.

In figure 7, segmentation results are shown on real medical images. First, right coronary arteries (RCA) are segmented. Second, left anterior descending

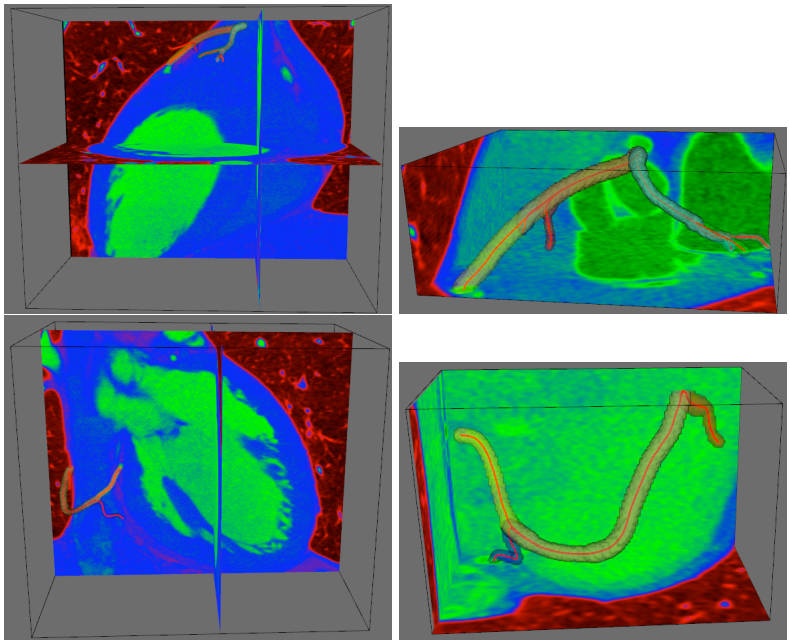

Fig. 7. First line : RCA segmentation using the tubular anisotropy approach shown on the whole image and on the selected sub-volume. Second line : LAD segmentation shown on the whole image and on the selected sub-volume. Only few points are required (the extremities of the paths). The tubular anisotropy method provides the centerline as well as vessels boundaries.

(LAD) arteries are segmented. One can see that the obtained radii on the principal coronary branches are larger than those of the secondary. Thus, our approach is robust to scale changing and bifurcations. Nevertheless, our current implementation requires huge memory allocations due to the 4D and anisotropic aspects. To overcome this issue, we added a pre-processing interactive tool to select a sub-volume containing the desired vessels (see figure 7). Moreover, we are working on a new implementation of the tubular anisotropy approach to make the memory allocation dynamic and hence to benefit from the front propagation aspect of the fast marching algorithm. Besides the reduction of the computation time (which has been actually achieved), we will save on memory allocation and will have a new version of our algorithm that extract the whole coronary arteries using a regular PC.

5 Conclusion and Perspective

In this paper we have proposed a new general method for tubular structure extraction in 2D and 3D images. Our method exploit the orientation of the vessels by using the optimally oriented flux to construct a multi-resolution anisotropic metric that describes the vessels orientation and scales. Combining this metric

with anisotropic minimal path technique, we are able to find a complete description of the tubular structure, i.e the centerline as well as the boundary. To summarize, our method is minimal interactive, robust to initialization, scale variations and bifurcations. In the future, we will work on a new implementation of our approach that makes the allocations dynamic. Then, the extraction of the whole coronary arteries will be possible on regular PC. Hence, we will be able to work on the medical validation of our approach.

Acknowledgement We would like to thank Professor Anthony J. Yezzi and Max Wai-Kong Law for interesting discussions. Also Eduardo Davila for his precious help for the implementation of the interface. Financial support was partially provided by ...

References

1. Sato, Y., Nakajima, S., Shiraga, N., Atsumi1, H., Yoshida, S., Koller, T., Gerig, G., Kikinis, R.: Three-dimensional multi-scale line filter for segmentation and visualization of curvilinear structures in medical images. MedIA **2**(2) (1998) 143–168
2. Krissian, K.: Flux-based anisotropic diffusion applied to enhancement of 3D angiogram. TMI **21**(11) (2002) 1440–1442
3. Frangi, R.F., Niessen, W.J., Vincken, K.L., Viergever, M.A.: Multiscale vessel enhancement filtering. Volume 1496., Springer-Verlag (1998) 130–137
4. Kirbas, C., Quek, F.K.H.: A review of vessel extraction techniques and algorithms. ACM Computing Surveys **36** (2004) 81–121
5. Deschamps, T., Cohen, L.: Fast extraction of minimal paths in 3D images and applications to virtual endoscopy. MIA **5**(4) (December 2001)
6. Cohen, L.D., Kimmel, R.: Global minimum for active contour models: a minimal path approach. International Journal of Computer Vision **24** (1997) 57–78
7. Jbabdi, S., Bellec, P., Toro, R., Daunizeau, J., Pélégrini-Issac, M., Benali, H.: Accurate anisotropic fast marching for diffusion-based geodesic tractography. Journal of Biomedical Imaging **2008**(1) (2008) 1–12
8. Li, H., Yezzi, A.: Vessels as 4D curves: Global minimal 4D paths to extract 3D tubular surfaces and centerlines. IEEE TMI **26**(9) (2007) 1213–1223
9. Law, M.W.K., Chung, A.C.S.: Three dimensional curvilinear structure detection using optimally oriented flux. ECCV **4** (2008) 368–382
10. Sethian, J.A., Vladimirsky, A.: Fast methods for the eikonal and related hamilton-jacobi equations on unstructured meshes. Proceedings of the National Academy of Sciences **97**(11) (May 2000) 5699–5703
11. Sethian, J.A.: A fast marching level set for monotonically advancing fronts. Proceedings of the National Academy of Sciences **93** (1996) 1591–1595
12. Tsitsiklis, J.N.: Efficient algorithms for globally optimal trajectories. IEEE Transactions on Automatic Control **40** (1995) 1528–1538
13. Chopp, D.L.: Replacing iterative algorithms with single-pass algorithms. Proc Nat Acad Sc USA **98**(20) (2001) 10992–10993
14. Lin, Q.: Enhancement, extraction, and visualization of 3D volume data. PhD thesis, Linkopings Universitet (2003)
15. Dijkstra, E.W.: A note on two problems in connection with graphs. Numerische Mathematic **1** (1959) 269–271